Electronic Supplementary Information (ESI)

Synthesis and characterization of uranyl(VI) complex with 2,6-pyridine-bis(methylaminophenolato) and its ligand-centred aerobic oxidation mechanism to diimino derivative

Tomoyuki Takeyama,[*,a] Satoshi Iwatsuki,[b] Satoru Tsushima,[c,d] Koichiro Takao[*,a]

AUTHOR ADDRESS

[a] Laboratory for Zero-Carbon Energy, Institute of Innovative Research, Tokyo Institute of Technology 2-12-1 N1-32, O-okayama, Meguro-ku, 152-8550 Tokyo, Japan

[b] Department of Chemistry, Konan University, Higashinada-ku, 658-8501 Kobe, Japan

[c] Institute of Resource Ecology, Helmholtz-Zentrum Dresden-Rossendorf (HZDR), Bautzner Landstraße 400, 01328 Dresden, Germany

[d] Tokyo Tech World Research Hub Initiative (WRHI), Institute of Innovative Research, Tokyo Institute of Technology, 2-12-1, O-okayama, Meguro-ku, 152-8550 Tokyo, Japan

Synthesis of ligands.

2,6-Bis[*N*-(3,5-di-*tert*-butyl-2-hydroxypheny)iminomethyl]pyridine (H_2(tBu-pdiop)).

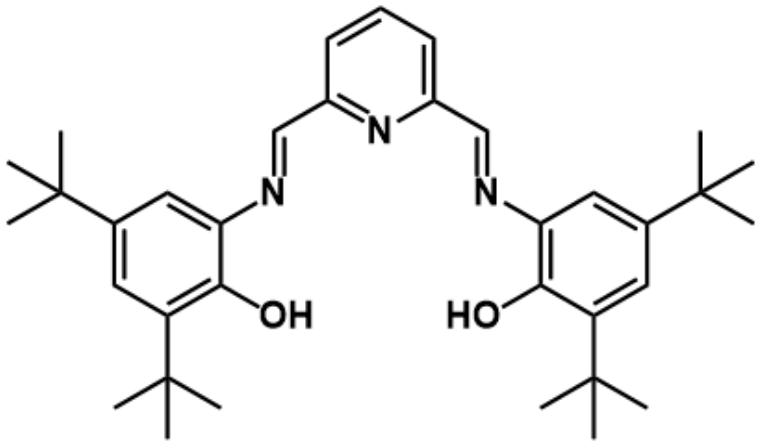

To an ethanol solution (10 mL) of 2-amino-4,6-di-*tert*-butylphenol (390.4 mg, 1.765 mmol) was added an ethanol solution (10 mL) of 2,6-pyridinedicarboxaldehyde (120.2 mg, 0.890 mmol). A yellow precipitate was formed within several minutes. This mixture was stirred for 2 h at room temperature. The yellow precipitate was collected by filtration and rinsed with ethanol. Recrystallization from CH_2Cl_2/ethanol yielded yellow needle crystals. Yield: 434.6 mg (91%). ^{1}H NMR spectrum recorded in $CDCl_3$ and IR spectrum are shown in Figures S1 and S2. ^{1}H NMR (399.78 MHz, $CDCl_3$, δ / ppm vs. TMS): 1.34 (s, 18H, -C(CH_3)$_3$), 1.47 (s, 18H, -C(CH_3)$_3$), 7.33 (d, 2H, aryl, $J_{H\text{-}H}$ = 2.0 Hz), 7.37 (d, 2H, aryl, $J_{H\text{-}H}$ = 2.4 Hz), 7.95 (t, 1H, py, $J_{H\text{-}H}$ = 7.6 Hz), 8.30 (d, 2H, py, $J_{H\text{-}H}$ = 7.6 Hz), 8.93 (s, 2H, -*H*C=N-). IR (ATR, cm^{-1}): 1583 (C=N stretching, $\nu_{C=N}$), 2867−2956 (CH_3 stretching, ν_{CH3}), 3070−3335 (O−H stretching, ν_{O-H}).

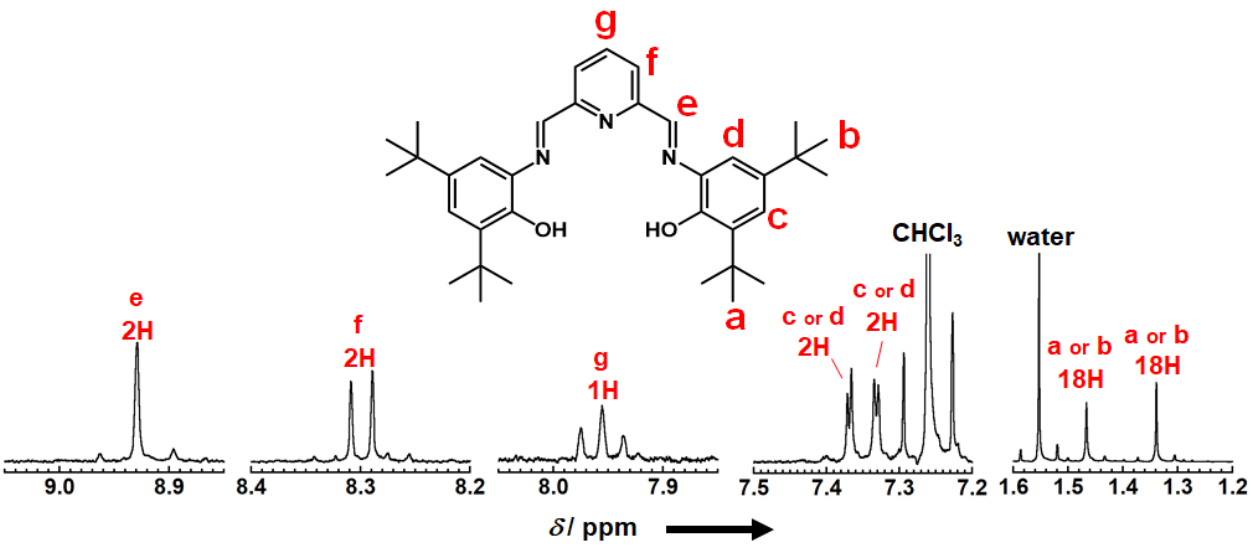

Figure S1. ^{1}H NMR spectrum of H_2(tBu-pdiop).

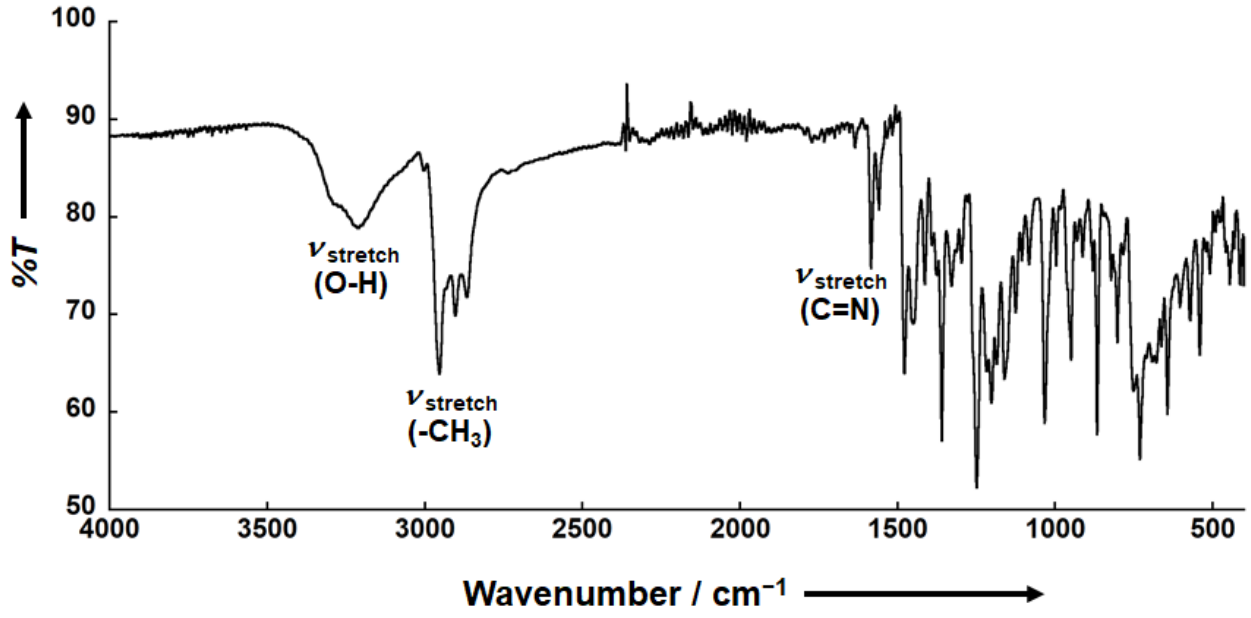

Figure S2. IR spectrum of H_2(tBu-pdiop).

2,6-Bis[*N*-(3,5-di-*tert*-butyl-2-hydroxyphenyl)aminomethyl]pyridine (H_2(tBu-pdaop)).

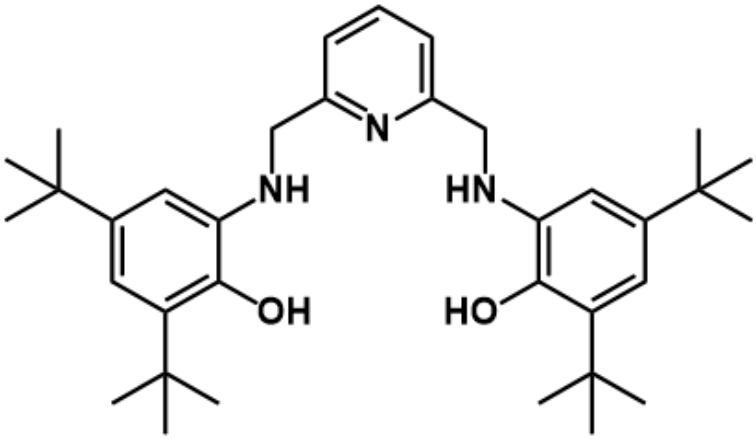

H_2(tBu-pdiop) (207.8 mg, 0.383 mmol) was dissolved in acetic acid (4 mL). Sodium borohydride (60 mg, 1.6 mmol) was added portionwise over a period of 40 min and this mixture was stirred for another hour at room temperature. The reaction was quenched by pouring it slowly in 200 mL of water. Extraction with CH_2Cl_2 (100 mL), subsequent drying of the organic phase over $MgSO_4$ and evaporation of the solvent afforded H_2(tBu-pdaop) as a pale yellow powder. Yield: 187.2 mg (90%). ^{1}H NMR spectrum recorded in $CDCl_3$ and IR spectrum are shown in Figures S3 and S4, respectively. ^{1}H NMR (399.78 MHz, $CDCl_3$, δ / ppm vs. TMS): 1.26 (s, 18H, -C(C*H*$_3$)$_3$), 1.43 (s, 18H, -C(C*H*$_3$)$_3$), 4.45 (s, 4H, -HN-C*H*$_2$-), 6.87 (d, 2H, aryl, $J_{H\text{-}H}$ = 2.0 Hz), 6.96 (d, 2H, aryl, $J_{H\text{-}H}$ = 2.0 Hz), 7.17 (d, 2H, py, $J_{H\text{-}H}$ = 7.6 Hz), 7.62 (t, 1H, py, $J_{H\text{-}H}$ = 7.6 Hz), 7.5-7.7 (br, 2H, -N*H*-). IR (ATR, cm^{-1}):, 2864−2950 (CH_3 stretching, ν_{CH3}), 3232 (N−H stretching, ν_{N-H}), 3514 (O−H stretching, ν_{O-H}).

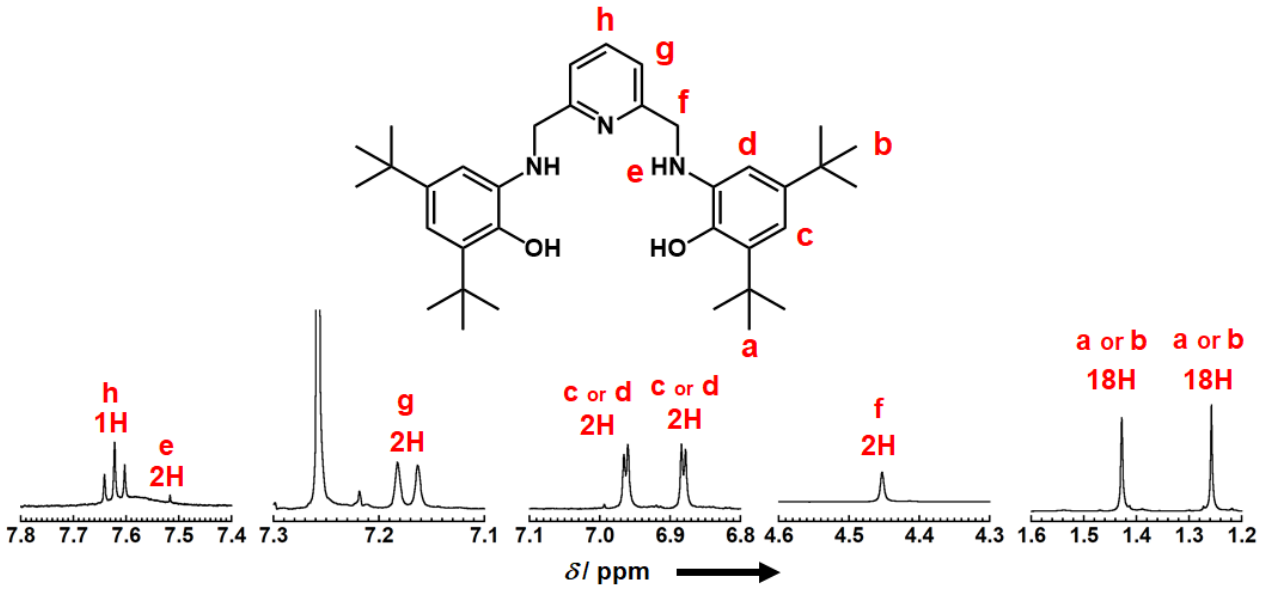

Figure S3. ^{1}H NMR spectrum of H_2(tBu-pdaop).

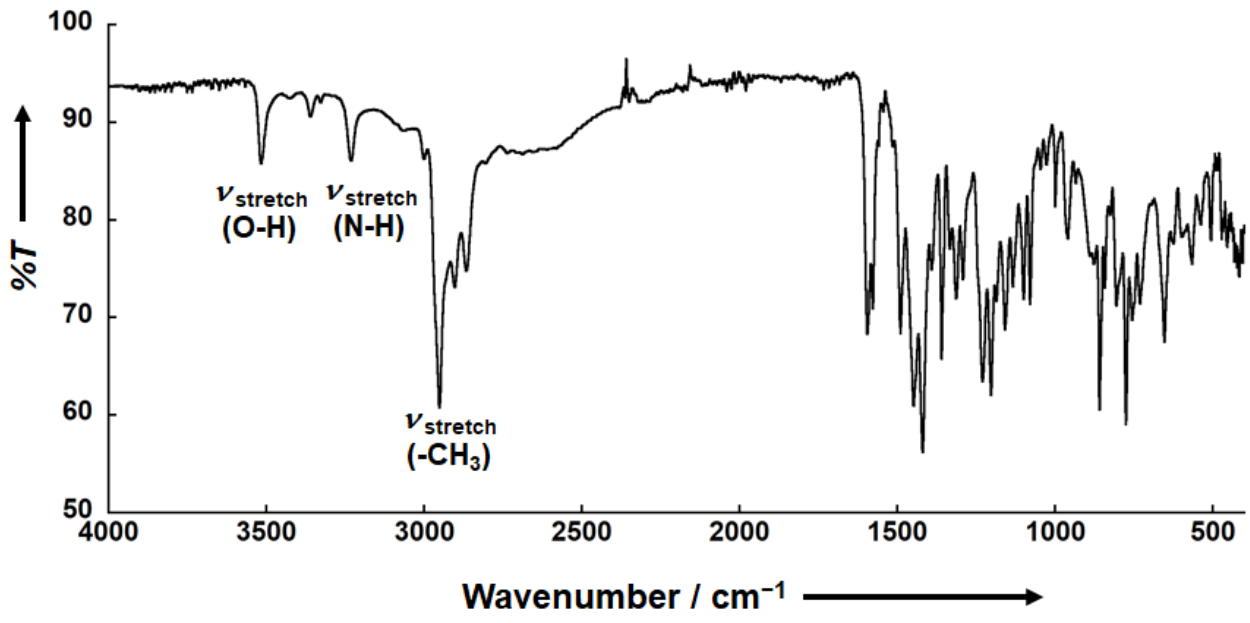

Figure S4. IR spectrum of H_2(tBu-pdaop).

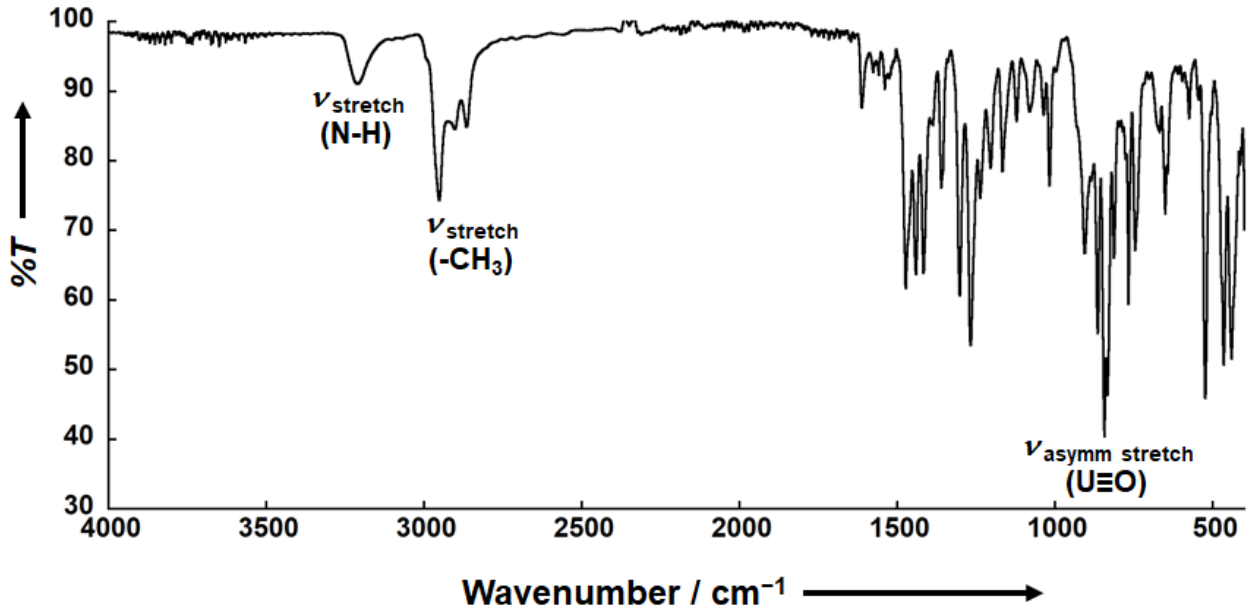

Figure S5. IR spectrum of UO_2(tBu-pdaop) (**1**).

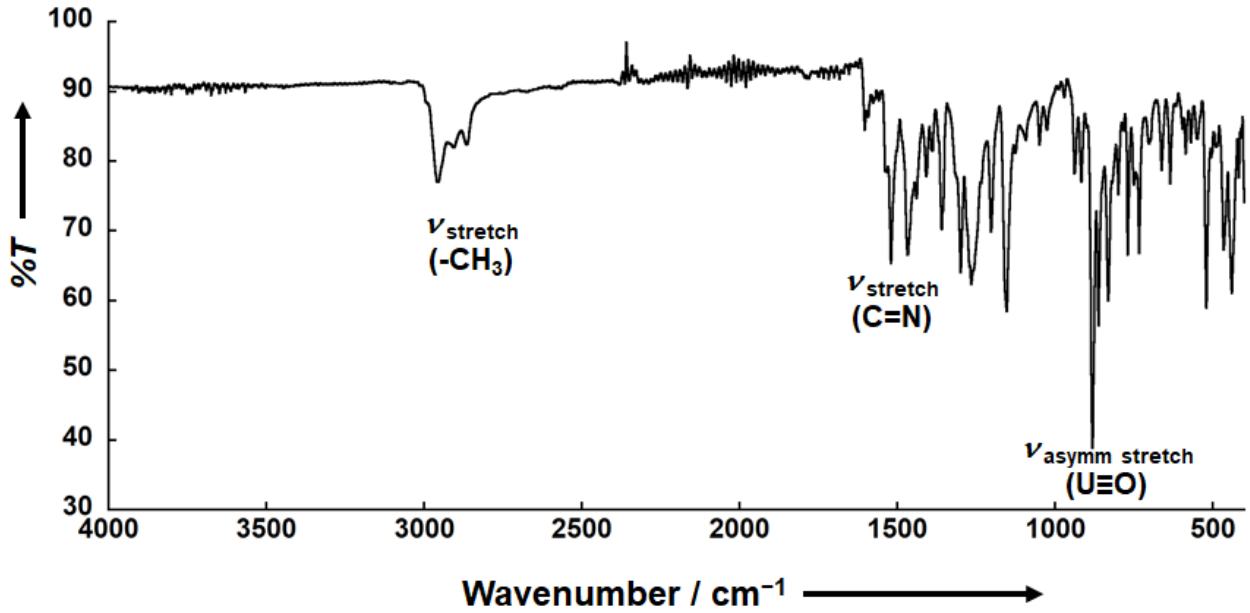

Figure S6. IR spectrum of UO_2(tBu-pdiop) (**2**).

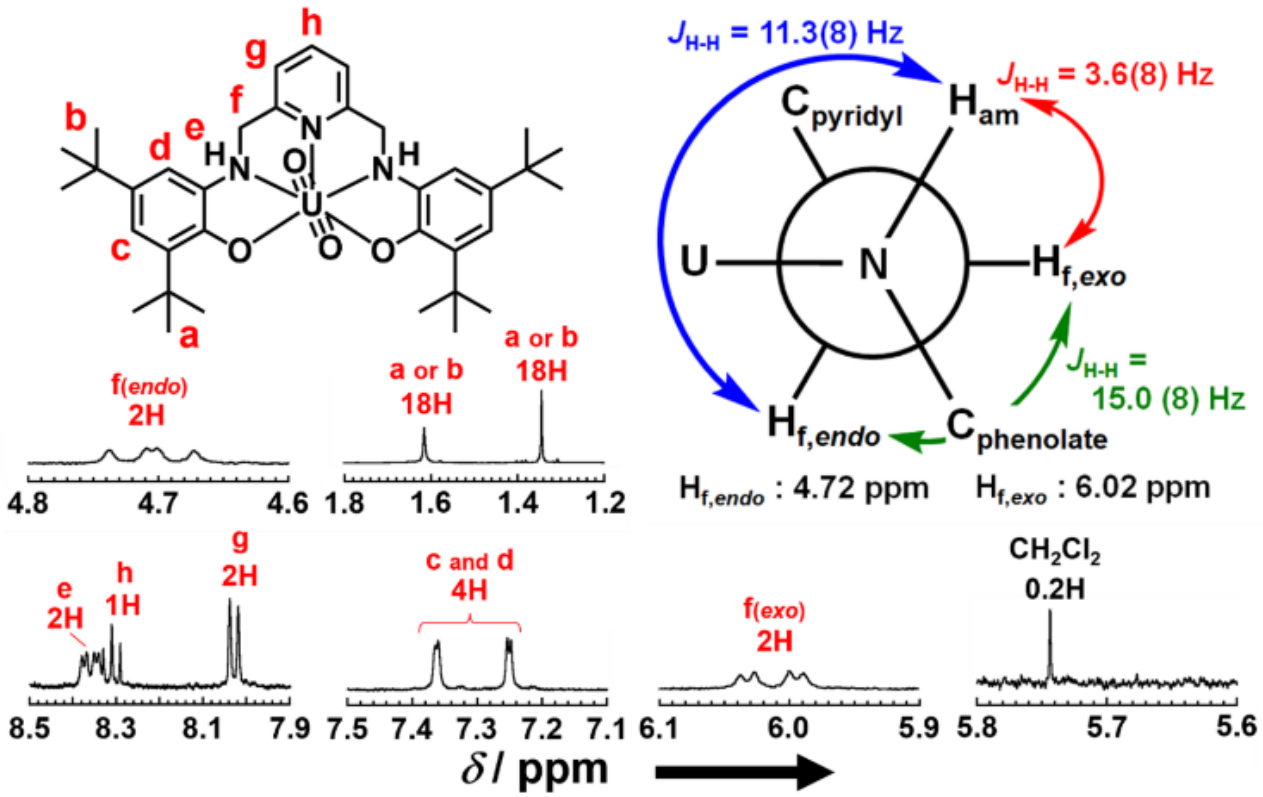

Figure S7. ^{1}H NMR spectrum of **1** in DMSO-d_6 at 298 K together with the molecular structure of **1** and Newman projection from amino N to methylene C.

Detailed description of crystallographic analysis.

The single crystals of complex **1** are very small needle crystals obtained from CH_2Cl_2/pentane recrystallized systems. Moreover, it should be emphasized that its crystallinity readily drops after picking it up from the mother liquor, because crystalline solvents included in this compound easily evaporates to destroy the crystal structure. This reason would be volatilization of crystalline solvents. Any trials of recrystallization from other solvents with lower volatilities like THF, pyridine, toluene, $CHCl_3$, and DMSO were unsuccessful. Therefore, we quickly mount a crystal on MiTeGen Dual Thickness MicroMounts, and set it on the temperature-controlled N_2 gas flow (123 K), immediately to collect good diffraction data. In unit cell of **1**·(CH_2Cl_2), highly disordered solvents molecules existed. Four CH_2Cl_2 molecules per unit cell (= one CH_2Cl_2 molecule per complex **1**) were actually found in the refinement process, and the atomic coordinates of this solvent molecule were determined. On the other hand, additional Q peaks and a solvent-accessible void were also observed. However, we could not find additional molecules in the crystal structure, because these molecules would be heavily disordered. Instead, the solvent masking routine in *Olex2* suggested that 252 electrons are present in a 684 $Å^3$ void in the unit cell. We also tested SQUEEZE program and obtained the similar result (a void of 788 $Å^3$ and 272 electrons per unit cell). These results imply that about six CH_2Cl_2 and/or pentane molecules exist in this crystal lattice. However, both solvent molecules, CH_2Cl_2 and pentane, coincidentally have 42 electrons, so that it would be difficult to distinguish them at this moment.

In spite of many trials for recrystallization and SCXRD experiments, some Alert level A and B are remained by check CIF report of International Union of Crystallography, as described below. The responses for these Alert are also described. To improve the large residual peaks around U atoms of **1**·(CH_2Cl_2), we applied the numerical absorption correction by using

indexed crystal faces. Even though, the large peaks around U atoms remained. No better results have been obtained in use of the empirical absorption correction with strong absorber options. When any absorption correction was not applied, the R_{int} values increased, indicating that absorption correction should be done. Despite these trials, the issue of residual peaks has not been resolved. Such an observation frequently occurs in a compound including a heavy atom.

_vrf_PLAT973;

PROBLEM: Check Calcd Positive Resid. Density on U1 5.48 eA-3

RESPONSE: We think that the insufficient or incorrect absorption correction is responsible of the residual densities. We applied the numerical absorption correction by using indexed crystal faces. Even though, the large peaks around U atoms remained. No better results have been obtained in use of the empirical absorption correction with strong absorber options. Despite many trials, we cannot correct this issue. Such an observation is frequently occurred in the compounds including a heavy atom.

_vrf_RINTA01;

PROBLEM: The value of Rint is greater than 0.18 Rint given 0.199

RESPONSE: The investigated single crystal was a small-sized, brittle and poorly diffracting needle. Numerous datasets were collected on single crystals from different batches, whereof the one of the highest quality is reported herein.

_vrf_PLAT020;

PROBLEM: The Value of Rint is Greater Than 0.12 Rint given 0.199

RESPONSE: The investigated single crystal was a small-sized, brittle and poorly diffracting needle. Numerous datasets were collected on single crystals from different batches, whereof the one of the highest quality is reported herein.

_vrf_PLAT342;

PROBLEM: Low Bond Precision on C-C Bonds 0.03441 Ang.

RESPONSE: The investigated single crystal was a small-sized, brittle and poorly diffracting needle. Numerous datasets were collected on single crystals from different batches, whereof the one of the highest quality is reported herein. However, such low precision in bond lengths had to appear due to weak diffractions and disordering atomic locations.

In crystallographic data of **2**·(C_5H_5N), some Alert level A and B are remained by check CIF report of International Union of Crystallography, as described below. The responses for these Alert are also described. To improve the large residual peaks around U atoms of **2**·(C_5H_5N), we applied the numerical absorption correction by using indexed crystal faces. Even though, the large peaks around U atoms remained. No better results have been obtained in use of the empirical absorption correction with strong absorber options. When any absorption correction was not applied, the R_{int} values increased, indicating that absorption correction should be done. Despite these trials, the issue of residual peaks has not been resolved. Such an observation frequently occurs in a compound including a heavy atom.

_vrf_PLAT971;

PROBLEM: Check Calcd Resid. Dens.	0.92A	From U1	7.13 eA-3
PROBLEM: Check Calcd Resid. Dens.	0.93A	From U1	6.94 eA-3
PROBLEM: Check Calcd Resid. Dens.	0.97A	From U1	4.07 eA-3
PROBLEM: Check Calcd Resid. Dens.	0.97A	From U1	4.03 eA-3
PROBLEM: Check Calcd Resid. Dens.	0.21A	From U1	3.33 eA-3

RESPONSE: We think that the insufficient or incorrect absorption correction is responsible of the residual densities. We applied the numerical absorption correction by using indexed crystal faces. Even though, the large peaks around U atoms remained. No better results have been obtained in use of the empirical absorption correction with strong absorber options. Despite many trials, we cannot correct this issue. Such an observation is frequently occurred in the compounds including a heavy atom.

_vrf_PLAT972;

PROBLEM: Check Calcd Resid. Dens.	0.81A	From U1	-4.93 eA-3
PROBLEM: Check Calcd Resid. Dens.	0.81A	From U1	-4.53 eA-3

RESPONSE: We think that the insufficient or incorrect absorption correction is responsible of the residual densities. We applied the numerical absorption correction by using indexed crystal faces. Even though, the large peaks around U atoms remained. No better results have been obtained in use of the empirical absorption correction with strong absorber options. Despite many trials, we cannot correct this issue. Such an observation is frequently occurred in the compounds including a heavy atom.

Sample preparation for kinetic measurements

The sample for kinetic measurements under ambient atmosphere condition were prepared by adding 3 mL of DMSO solution dissolved **1** (concentration of **1** (C_1^{ini}) = 0.10 mM) and 1 mL of air in a 10-mm quartz cell. Immediately after sample preparation, absorbance spectral changes with time was monitored by spectrophotometer.

The sample for kinetic measurement under the O_2-saturated condition was prepared by following procedure. The O_2-saturated DMSO was prepared by purging O_2 gas into DMSO overnight. Sample cell (10-mm quartz cell of 4 mL volume) was also purged with O_2 gas before use. Sample was prepared by dissolving complex **1** in O_2-saturated DMSO (C_1^{ini} = 0.10 mM) and 3 mL was put into cell which was then purged with O_2. Immediately after sample preparation, absorbance change with time at 515 nm at 293 K was monitored by spectrophotometer.

The sample for kinetic measurement under the Ar atmosphere was prepared by following procedure. The deoxygenized DMSO was purchased from FUJIFILM Wako Chemicals Corporation. Complex **1** was dissolved in the deoxygenized DMSO (C_1^{ini} = 0.10 mM, 3 mL) under Ar atmosphere. After adding the solution in the sample cell (10-mm quartz cell of 4 mL), it was sealed under Ar atmosphere. Immediately after removing the sample cell from Ar atmosphere, absorbance change with time at 515 nm at 293 K was monitored by spectrophotometer.

The sample for kinetic measurements of reaction **1-*d*$_4$** under the ambient atmosphere condition was prepared by similar manner to that of reaction **1** under the ambient atmosphere condition.

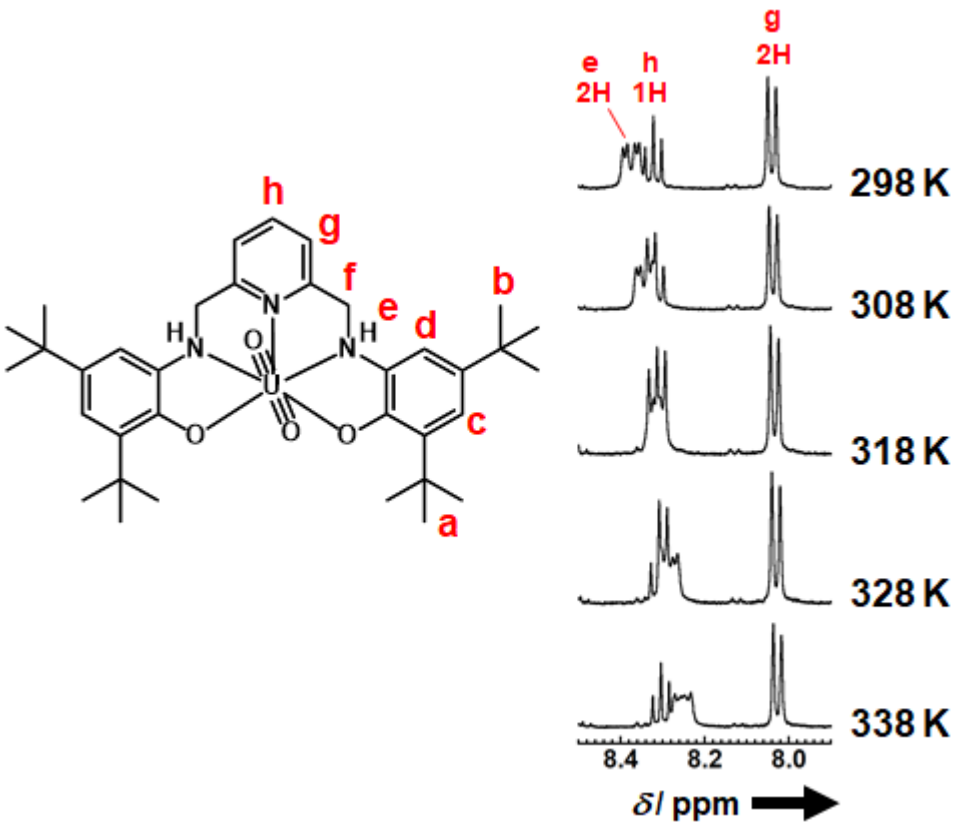

Figure S8. ^{1}H NMR spectrum of **1** in DMSO-d_6 recorded at various temperatures.

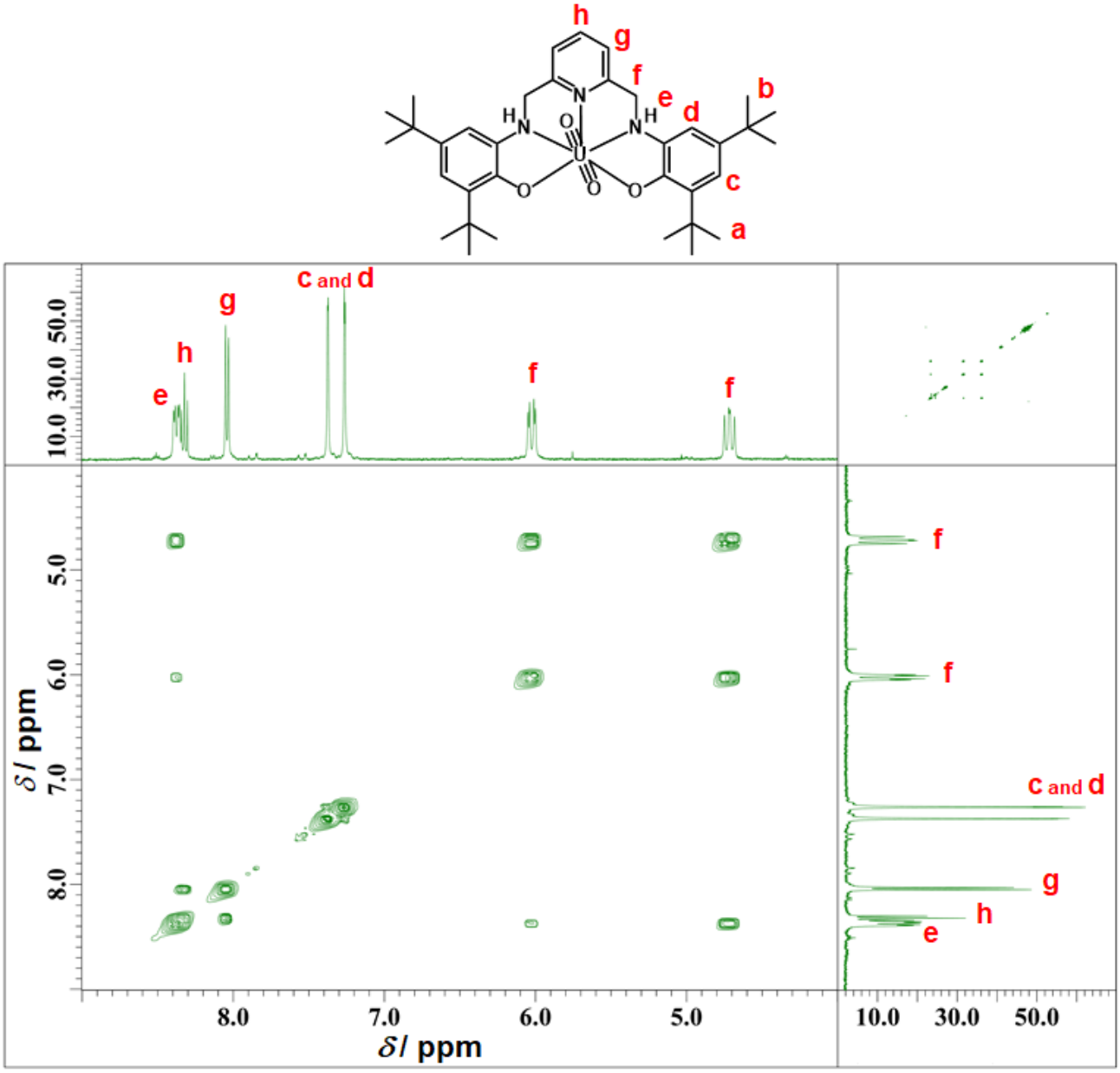

Figure S9. ^{1}H-^{1}H COSY diagram of **1** in DMSO-d_6 at 298 K

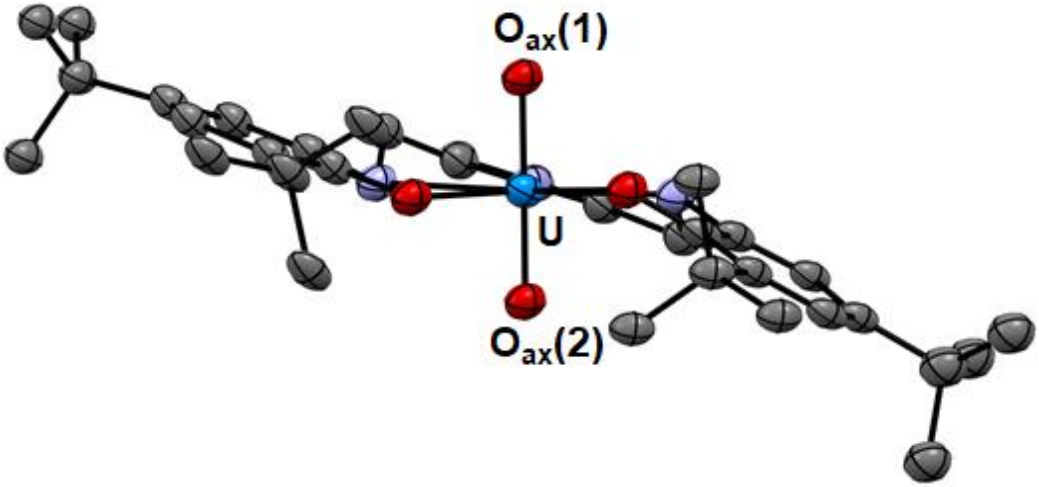

Figure S10. ORTEP views of **1**. Ellipsoids are at 30% probability. Hydrogen atoms, solvents molecules were omitted for clarity.

Table S1. Selected bond lengths (Å) and bond angles (º) of **1**·(CH_2Cl_2).

Selected bond lengths (Å)			
U(1)−O(1)	1.77(1)	C(1)−O(3)	1.35(3)
U(1)−O(2)	1.74(1)	C(19)−O(4)	1.34(3)
U(1)−O(3)	2.19(2)	C(7)−N(1)	1.53(3)
U(1)−O(4)	2.22(2)	C(13)−N(3)	1.38(3)
U(1)−N(1)	2.60(2)	C(6)−N(1)	1.47(2)
U(1)−N(2)	2.55(2)	C(14)−N(3)	1.52(4)
U(1)−N(3)	2.56(2)		
Selected bond angles (º)			
C(6)−N(1)−C(7)	111(2)	C(13)−N(3)−C(14)	115(2)
C(6)−N(1)−U(1)	109(1)	C(13)−N(3)−U(1)	109(1)
C(7)−N(1)−U(1)	114(1)	C(14)−N(3)−U(1)	106(1)

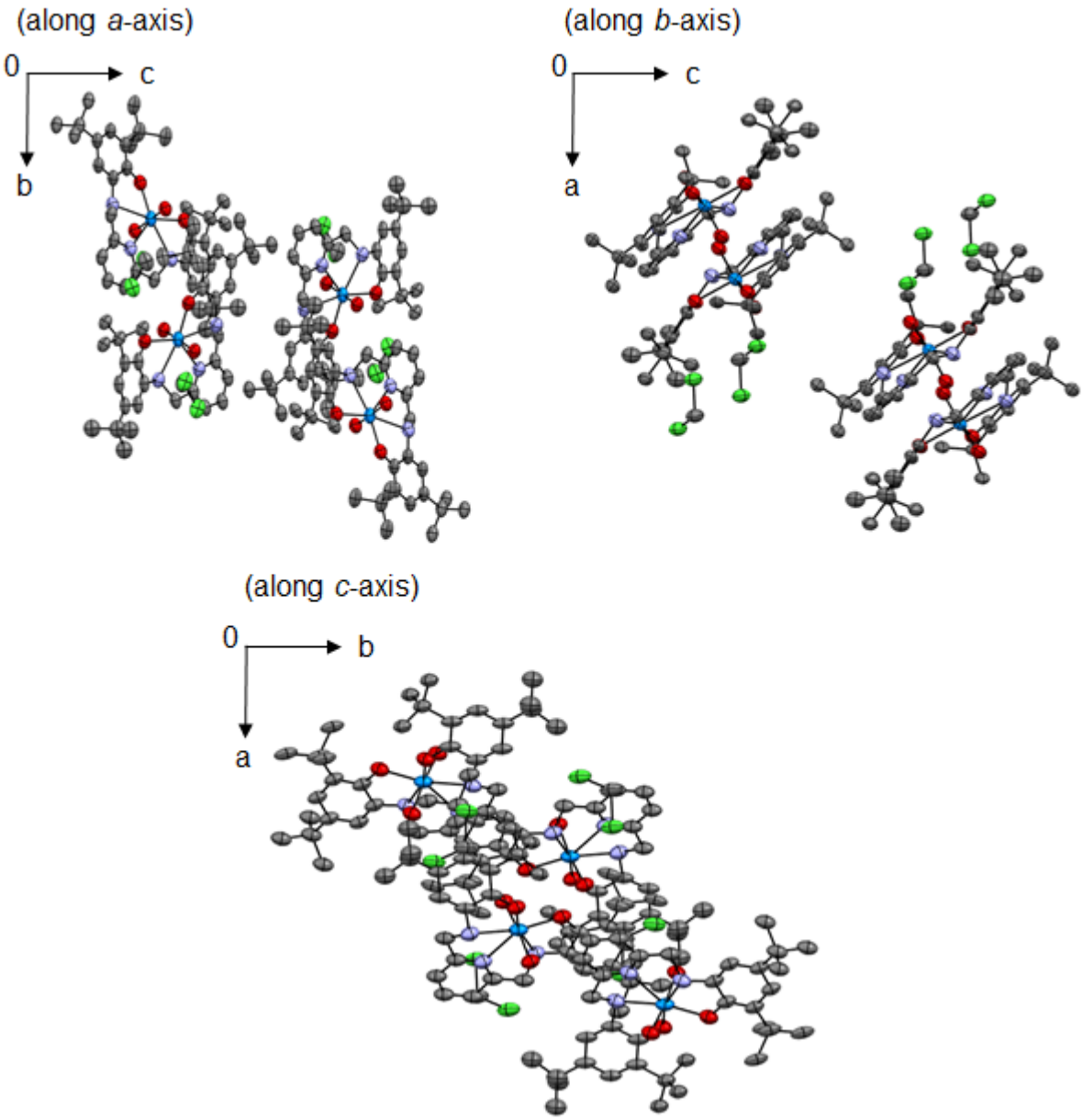

Figure S11. Crystal packing of **1**·(CH_2Cl_2). Ellipsoids are at 30% probability. Hydrogen atoms were omitted for clarity. The meaningful interaction between the molecules of **1** is not observed. On the other hand, O_{ax} atom of UO_2^{2+} interacts with H atom of a CH_2Cl_2 molecule (2.37 Å) which is crystalline solvent.

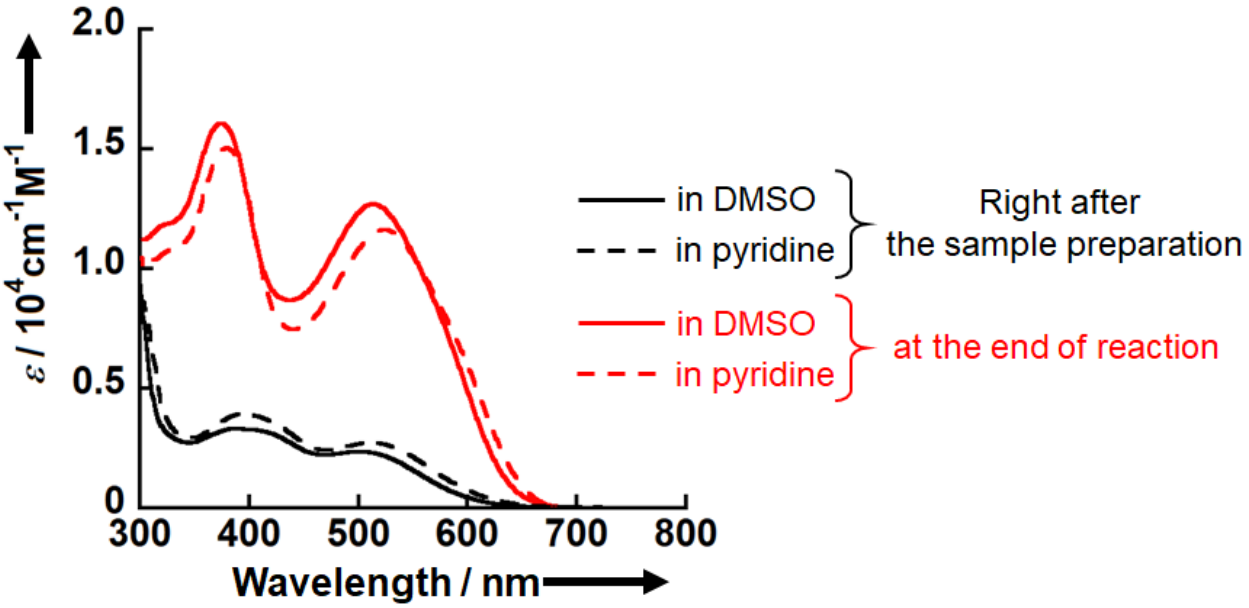

Figure S12. Absorbance spectra of **1** right after the sample preparation (black) and at the end of the reaction (red). Solid and dashed lines represent the DMSO-d_6 and pyridine solutions, respectively.

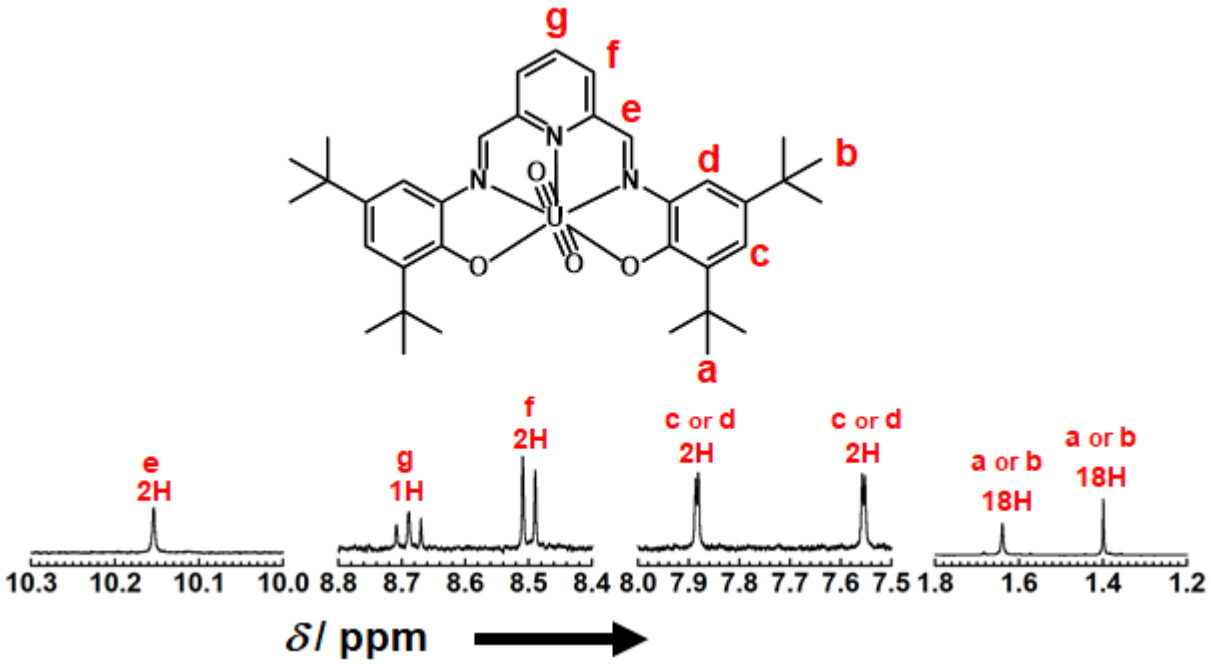

Figure S13. ^{1}H NMR spectra of the DMSO-d_6 solution of **1** 60 hours after preparation and signal assignments.

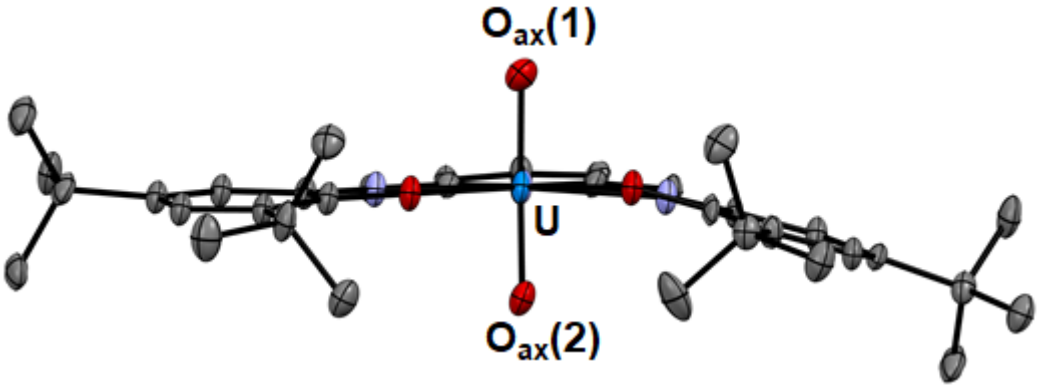

Figure S14. ORTEP views of **2**. Ellipsoids are at 50% probability. Hydrogen atoms, solvents molecules were omitted for clarify.

Table S2. Selected bond lengths (Å) and bond angles (º) of **2**·(C_5H_5N).

Selected bond lengths (Å)			
U(1)−O(1)	1.773(6)	C(1)−O(3)	1.324(9)
U(1)−O(2)	1.761(5)	C(19)−O(4)	1.33(1)
U(1)−O(3)	2.240(7)	C(7)−N(1)	1.29(1)
U(1)−O(4)	2.231(6)	C(13)−N(3)	1.27(1)
U(1)−N(1)	2.579(7)	C(6)−N(1)	1.40(1)
U(1)−N(2)	2.533(8)	C(14)−N(3)	1.41(1)
U(1)−N(3)	2.565(8)		
Selected bond angles (º)			
C(6)−N(1)−C(7)	124.9(7)	C(13)−N(3)−C(14)	124.3(7)
C(6)−N(1)−U(1)	114.8(5)	C(13)−N(3)−U(1)	120.6(6)
C(7)−N(1)−U(1)	120.3(6)	C(14)−N(3)−U(1)	115.1(5)

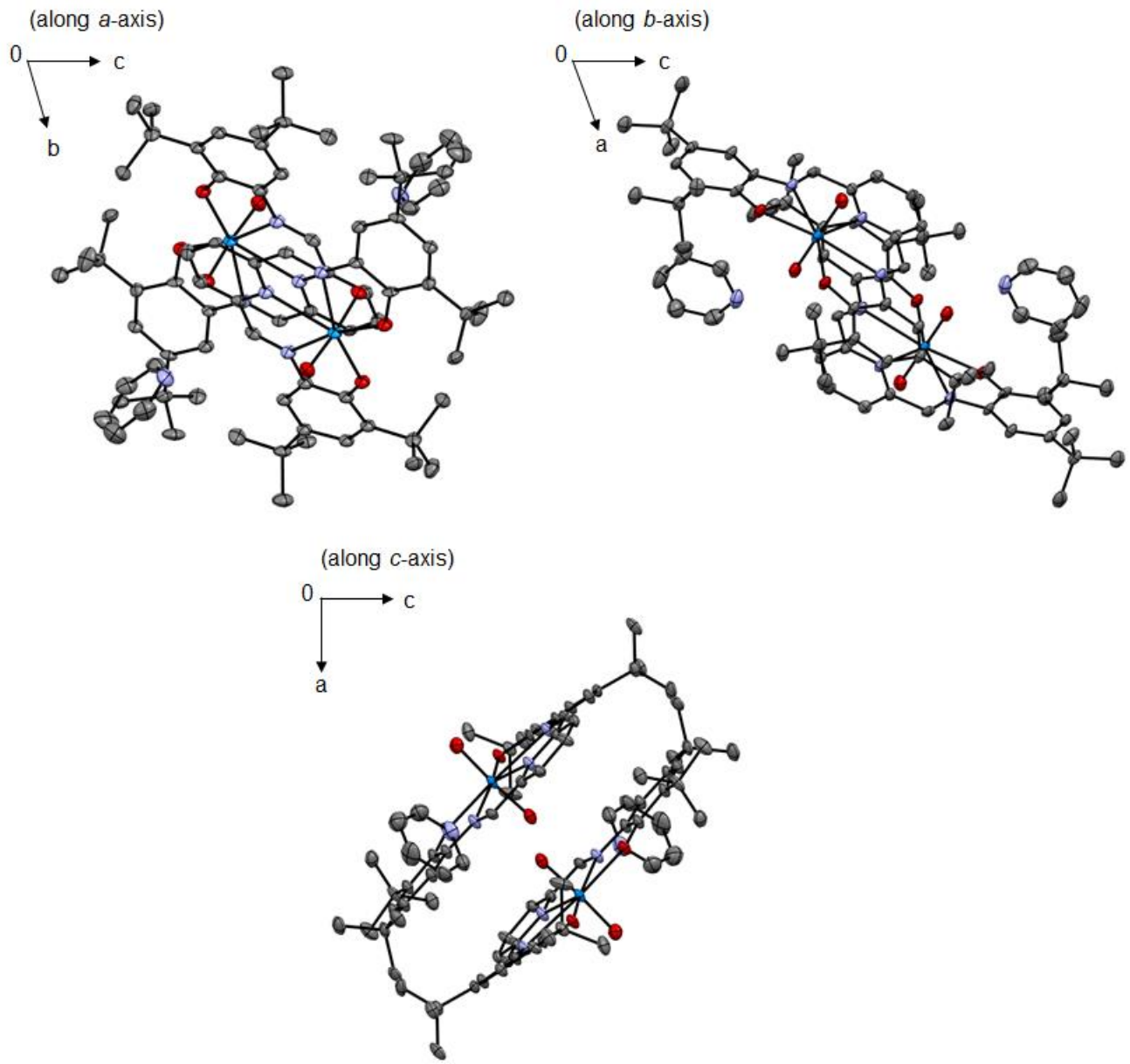

Figure S15. Crystal packing of **2**·(C_5H_5N). Ellipsoids are at 30% probability. Hydrogen atoms were omitted for clarity. The meaningful interaction between the molecules of **2** is not observed. On the other hand, O_{ax} atom of UO_2^{2+} interacts with H atom of a pyridine molecule (2.44 Å) which is crystalline solvent. Packing structure of **2**·(C_5H_5N) is different from that of **1**·(CH_2Cl_2). The difference in their packing structures arises from the difference in planarity of complex **1** and **2**. From the Figure S10 and S 14, the planarity of complex **1** in crystal is relatively lower than that of complex **2**. Moreover, the crystalline solvents in crystals of complex **1** and **2** would affects the packing structures.

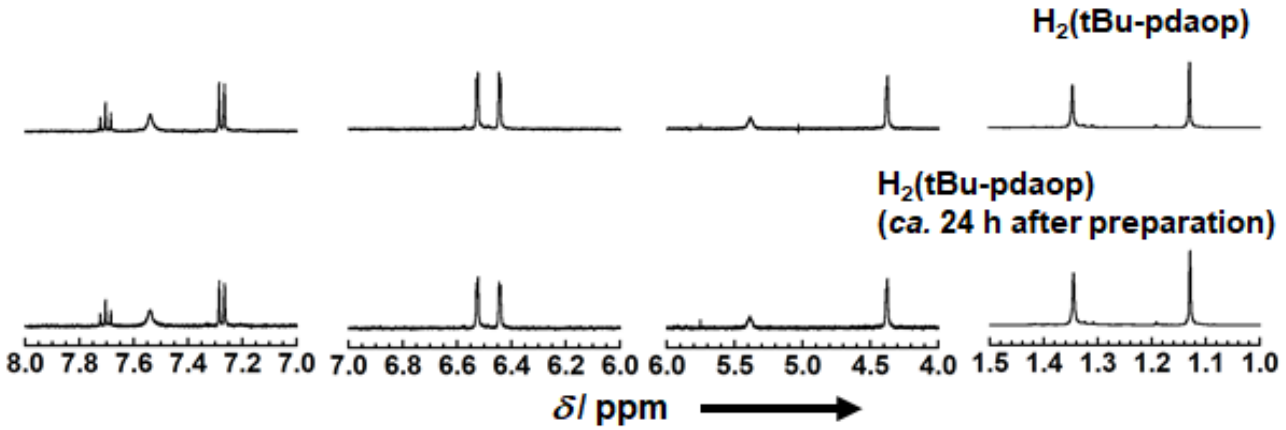

Figure S16. ^{1}H NMR spectra of the DMSO-d_6 solution of H_2(tBu-pdaop) 0 and 24 hours after preparation.

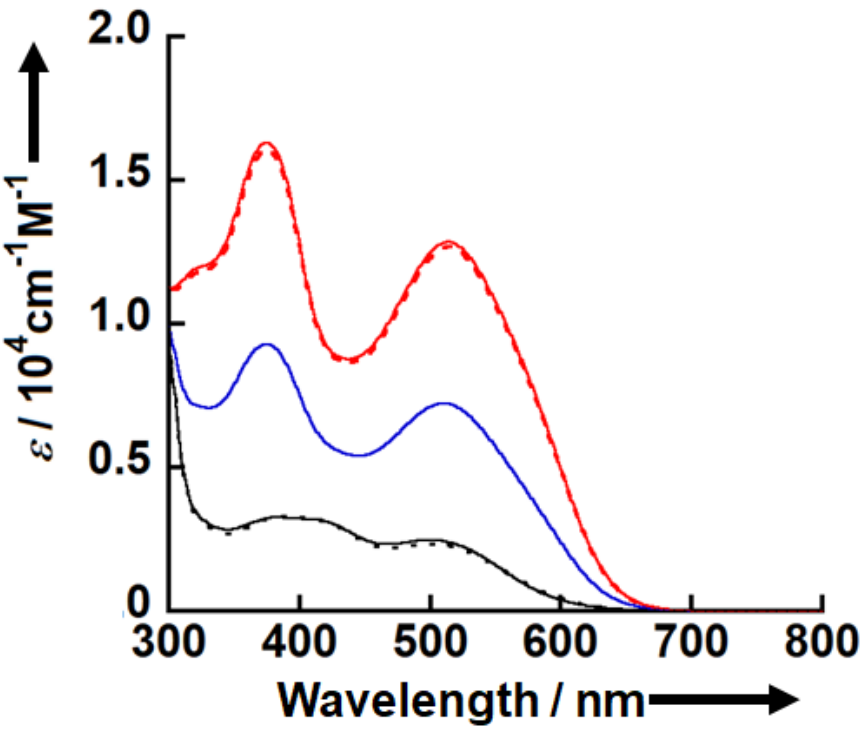

Figure S17. The calculated spectra of the starting complex (black solid line), the intermediate complex generated in the first step (blue), and the final product complex (red solid line), obtained from the SPECTFIT analysis for Figure 5(a). The dash lines represent the experimental results (black; initial spectrum, red; final spectrum in Figure 5(a))

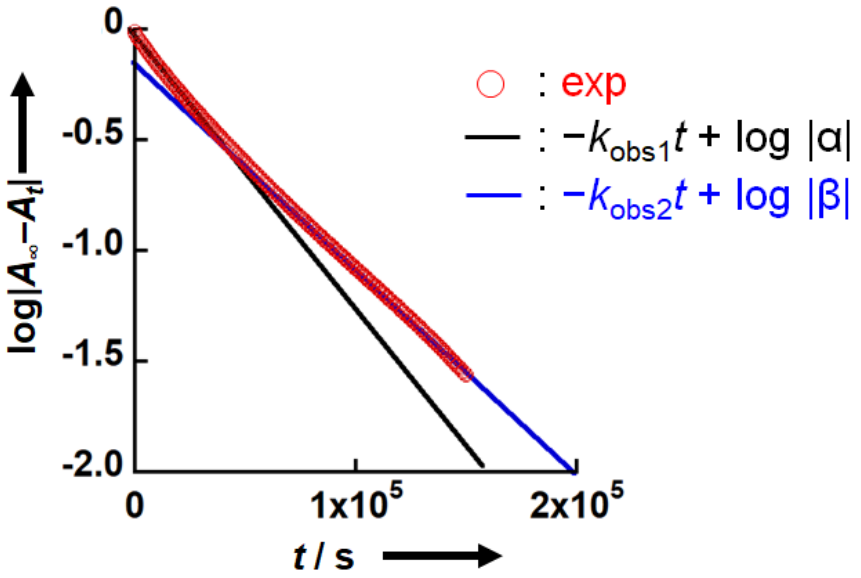

Figure S18. The plot of log $|A_\infty - A_t|$ against time of the oxidation of **1** (0.10 mM) in DMSO under ambient atmosphere at 293K. Two different slopes in the progress of the reaction indicate that the reaction proceeds with consecutive two-step (pseudo) first-order kinetics.

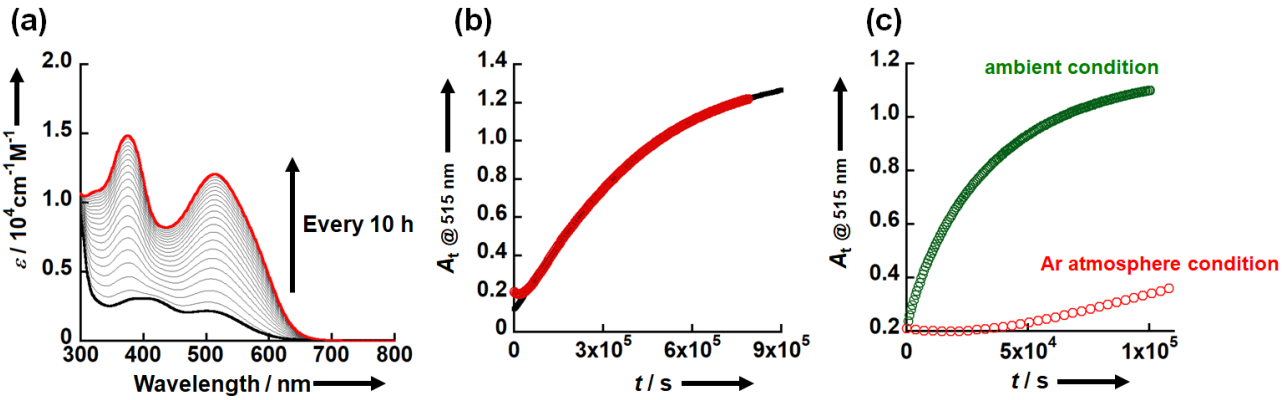

Figure S19. Time-resolved UV-vis absorption spectra through the oxidation of **1** (0.10 mM) in DMSO under Ar atmosphere condition at 293 K (a). The spectra were represented by 10 h intervals. Absorbance changes at 515 nm with time is shown in panel (b). A Black line in panel (b) represents the best fit assuming the first-order two-step kinetics model. The difference of absorbance changes at 515 nm with time under the ambient atmosphere (green circles) and Ar atmosphere condition (red circles) is shown in panel (c)

Table S3. Conditional pseudo first order rate constants (k_{obs1} and k_{obs2}) for the reaction of **1** and **1-*d*$_4$** with O_2 under various conditions.

T / K	C_1^{ini} / mM[a]	k_{obs1} / $10^{-4}s^{-1}$	k_{obs2} / $10^{-5}s^{-1}$
ambient atmosphere (p_{O2} = 0.21 atm)			
293	0.10	0.72	2.18
303	0.10	1.37	4.22
313	0.10	4.55	13.8
323	0.10	8.34	24.7
333	0.10	15.3	52.5
O_2 saturated condition (p_{O2} = 1 atm)			
293	0.10	0.76	1.80
Ar atmosphere condition			
293	0.10	0.192	0.251
The oxidation of **1-*d*$_4$** under the ambient atmosphere (p_{O2} = 0.21 atm)			
313	0.10	1.23 (KIE =3.7)	2.80 (KIE = 4.9)

[a] Initial concentration of **1**

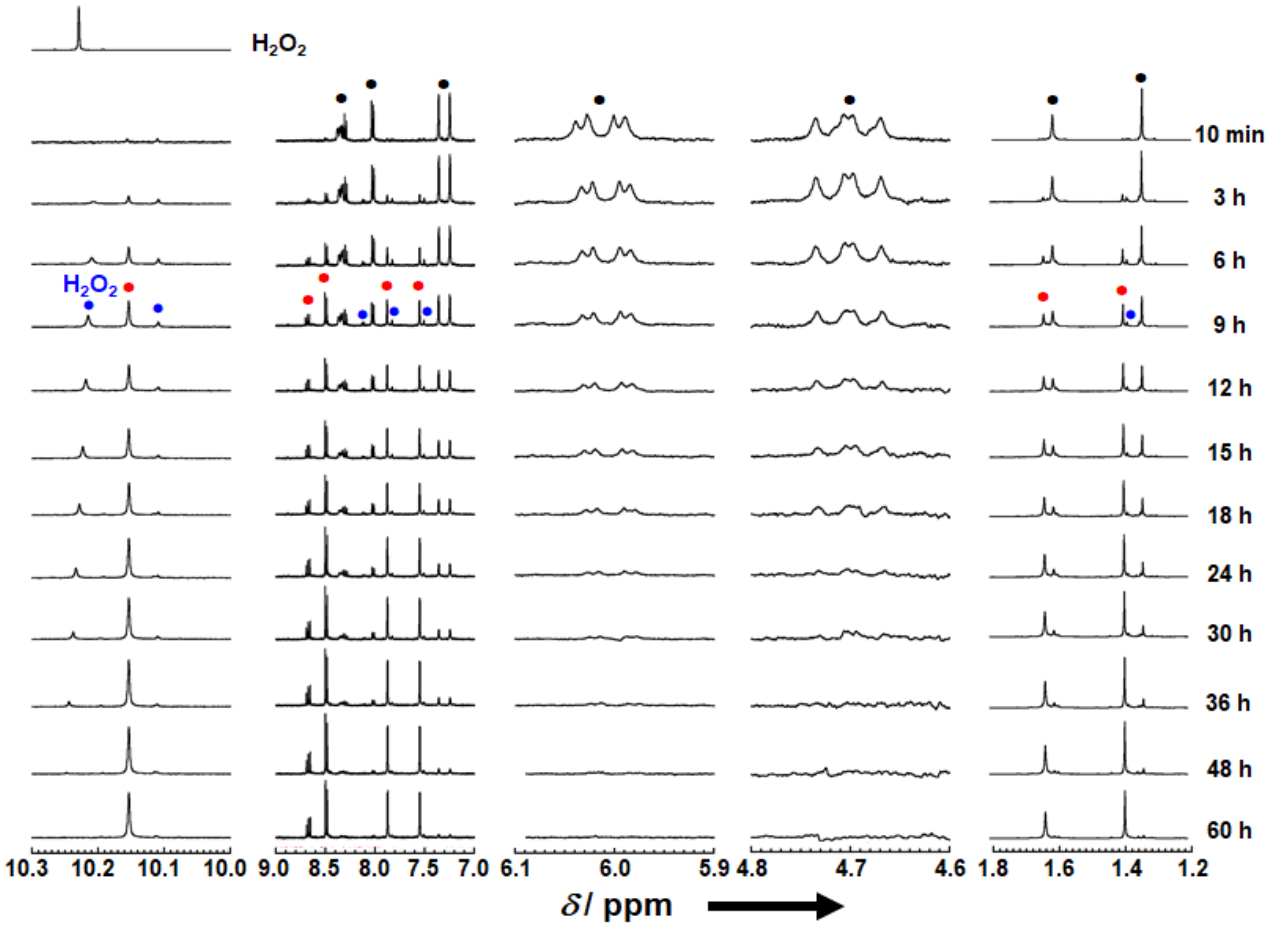

Figure S20. ^{1}H NMR spectra of the DMSO-d_6 solution of **1** 10 minutes, 3, 6, 9, 12, 15, 18, 24, 30, 36, 48, and 60 hours after preparation. Black, red, and blue circles represent the signals of **1**, **2**, and **1'**, respectively.

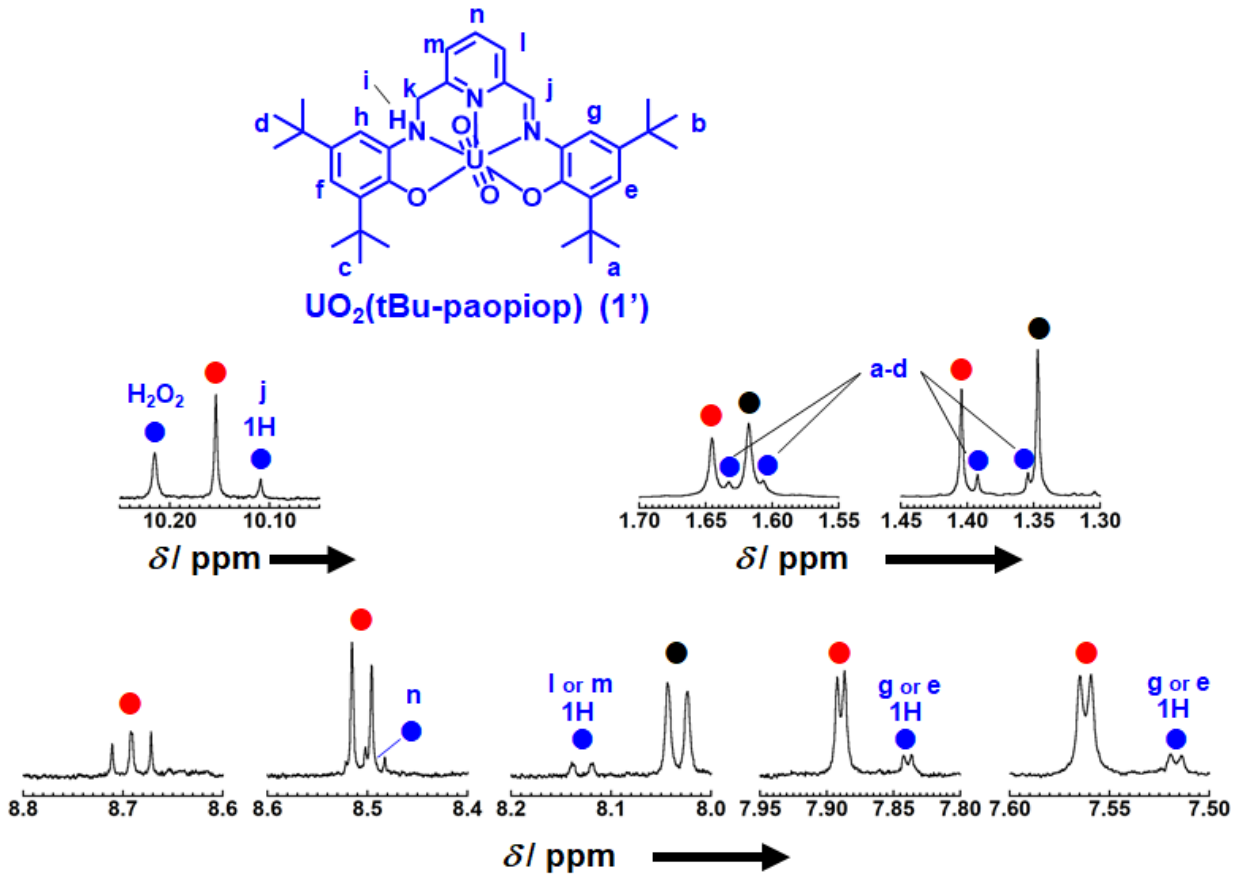

Figure S21. ^{1}H NMR spectra of the DMSO-d_6 solution of **1** 9 hours after preparation. Black, red, and blue circles represent the signals of **1**, **2**, and **1'** plus H_2O_2, respectively. Some signals of **1'** were not clearly observed due to superposition of signals of other species.

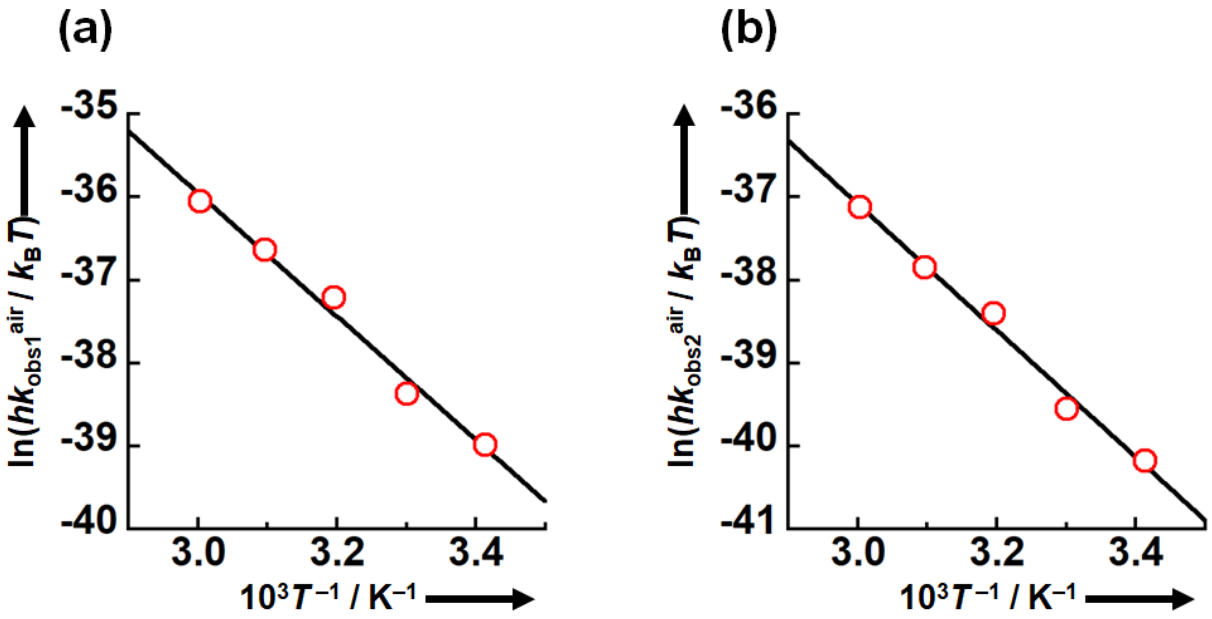

Figure S22. Eyring plot of k_{obs1} (a) and k_{obs2} (b) of the oxidation of **1** (0.10 mM) in DMSO under ambient atmosphere. Black line represents the theoretical fitting line.

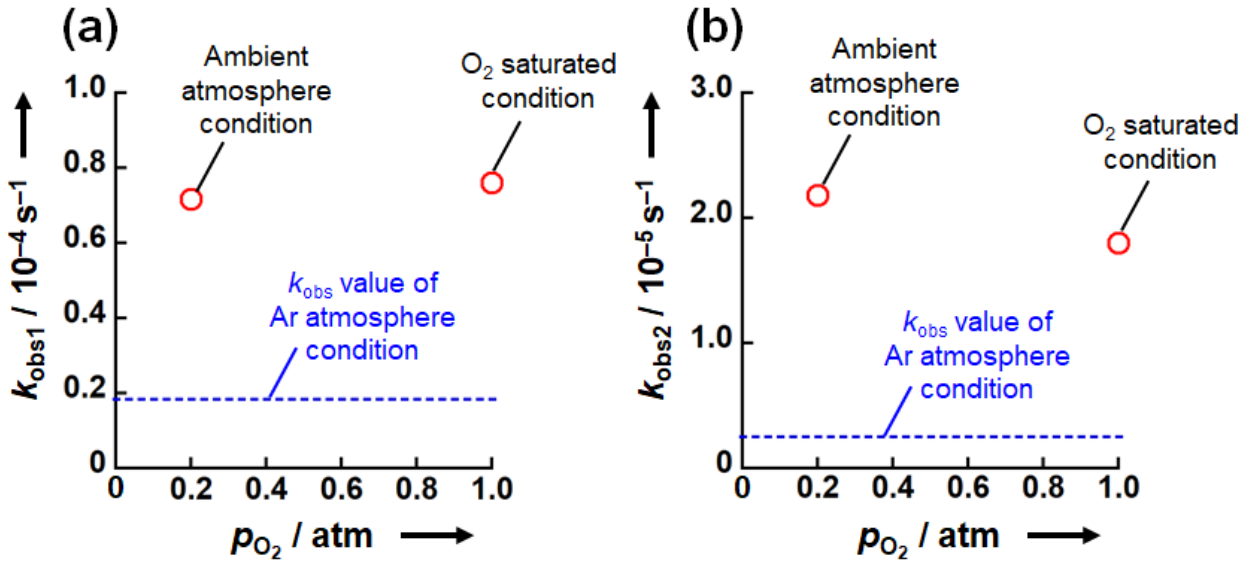

Figure S23. The dependence of k_{obs1} (a) and k_{obs2} (b) on the O_2 partial pressure (p_{O2}) for the oxidation of **1**. Blue dash line represents the experimental of k_{obs1} and k_{obs2} values of Ar atmosphere condition.

Synthesis of deuterated UO_2(tBu-pdaop) complex (UO_2(tBu-pdaop-*d*$_4$)).

2,6-Bis[*N*-(3,5-di-*tert*-butyl-2-hydroxyphenyl)aminomethyl]pyridine-*d*$_4$ (D_2(tBu-pdaop-*d*$_4$)).

H_2(tBu-pdiop) (110.0 mg, 0.203 mmol) was dissolved in acetic acid-*d*$_4$ (4 mL). Sodium borodeuteride (40 mg, 0.96 mmol) was added portion wise over a period of 40 min. Methanol-*d*$_4$ (0.5 mL) was added to the reaction mixture. This mixture was stirred for 30 min at room temperature. The reaction was quenched by pouring it slowly in 15 mL of D_2O. Extraction with dried CH_2Cl_2 (20 mL), subsequent drying of the organic phase over $MgSO_4$ and evaporation of the solvent afforded D_2(tBu-pdaop-*d*$_4$) as a white powder. Yield: 83.0 mg (74%). ^{1}H NMR (399.78 MHz, $CDCl_3$, δ / ppm vs. TMS): 1.26 (s, 18H, -C(C*H*$_3$)$_3$), 1.43 (s, 18H, -C(C*H*$_3$)$_3$), 4.43 (s, 2H, -HN-C*H*$_2$-), 6.88 (d, 2H, aryl, $J_{H\text{-}H}$ = 2.4 Hz), 6.96 (d, 2H, aryl, $J_{H\text{-}H}$ = 2.4 Hz), 7.17 (d, 2H, py, $J_{H\text{-}H}$ = 7.6 Hz), 7.62 (t, 1H, py, $J_{H\text{-}H}$ = 7.6 Hz).

UO_2(tBu-pdaop-*d*$_4$) (1-*d*$_4$). To a solution of $UO_2(CH_3COO)_2{\cdot}2H_2O$ (20.8 mg, 49.0 μmol) in deoxygenized methanol-*d*$_4$ (2 mL) was added a solution of D_2(tBu-pdaop-*d*$_4$) (27.5 mg, 50.0 μmol) in deoxygenized CH_2Cl_2 (2 mL) under Ar. This violet solution was stirred at –40°C for 15 min. Evaporation of the solvent afforded UO_2(tBu-pdaop-*d*$_4$) as a violet powder. It was quickly collected by filtration, and rinsed with hexane. Yield: 32.2 mg (81%). The deuteration ratio of the C–D bond of α-carbon of amine and N–D bond of amine moieties was estimated to be 94 % by NMR spectroscopy. This compound was characterized by ^{1}H NMR, and IR. ^{1}H NMR (399.78 MHz, CD_2Cl_2, δ / ppm vs. TMS): 1.42 (s, 18H, -C(C*H*$_3$)$_3$), 1.69 (s, 18H, -C(C*H*$_3$)$_3$), 5.06 (br, 1H, -CH_2-), 5.92 (br, 1H, -CH_2-), 6.26 (br, 0.12H, -N*H*-), 7.41 (s, 2H, aryl), 7.48 (d, 2H, aryl, $J_{H\text{-}H}$ = 2.4 Hz), 7.87 (d, 2H, py, $J_{H\text{-}H}$ = 7.6 Hz), 8.18 (t, 1H, py, $J_{H\text{-}H}$ = 8.0 Hz) (Figure S24). IR (ATR, cm^{-1}): 861 (O≡U≡O asymmetric stretching, ν_3).

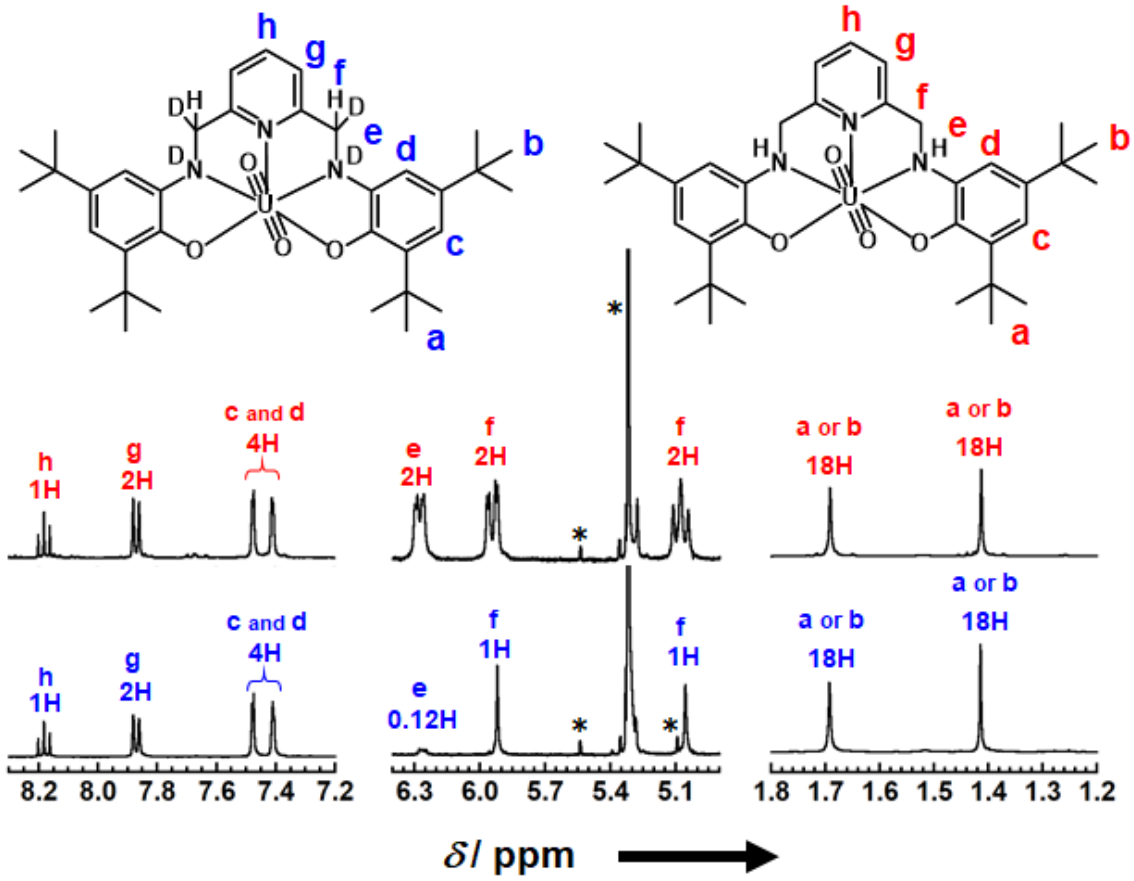

Figure S24. ^{1}H NMR spectra of **1** (top) and **1-*d*$_4$** (bottom) in CD_2Cl_2. ∗ is represent as the solvent signals (CH_2Cl_2).

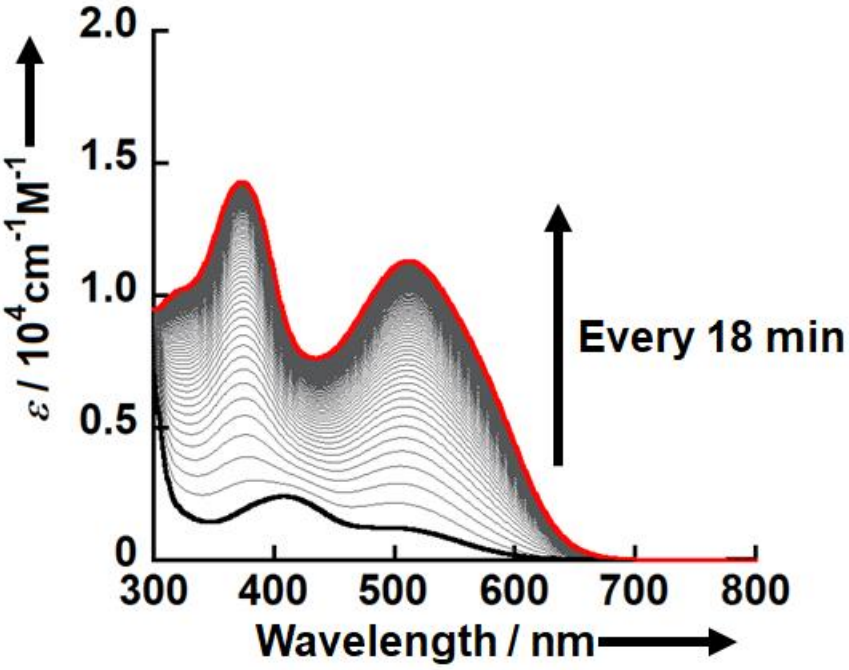

Figure S25. Absorption spectral changes with time for the oxidation of **1-*d*$_4$** (0.10 mM) in DMSO under the ambient atmosphere at 313 K. The spectra were represented by 18 min intervals.

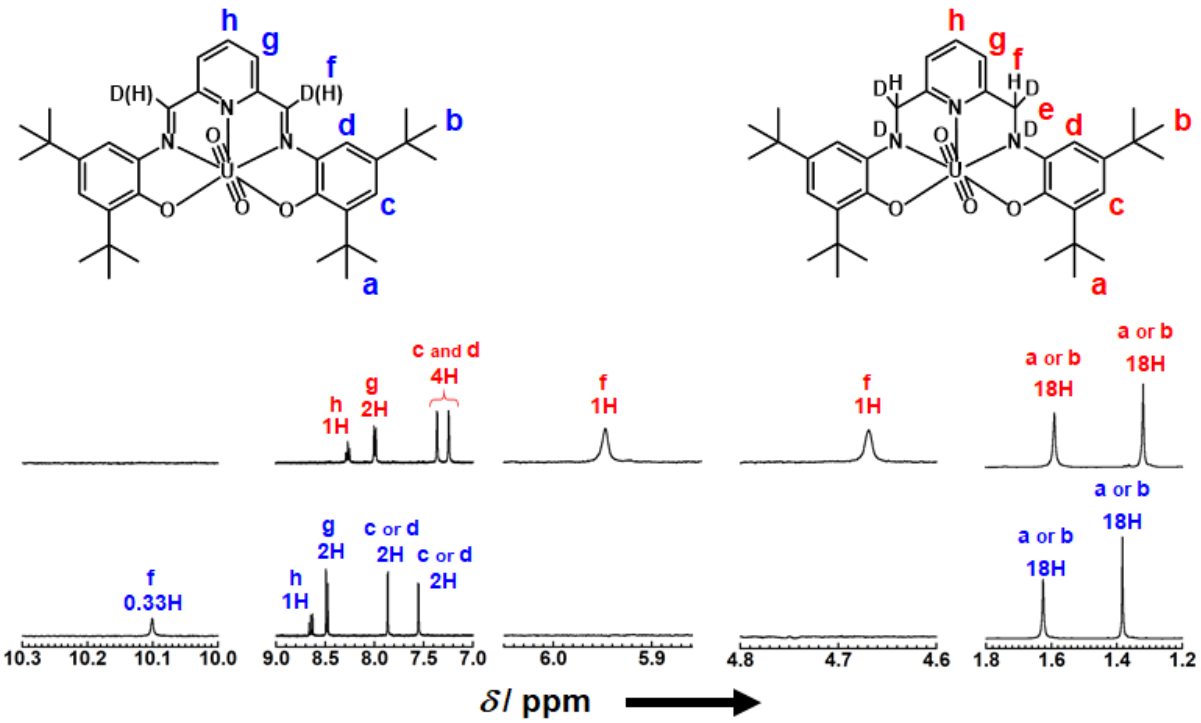

Figure S26. ^{1}H NMR spectra of the DMSO-d_6 solution of **1-*d*$_4$** (top) and sample solution heated at 353 K for 3 hours after preparation (bottom).

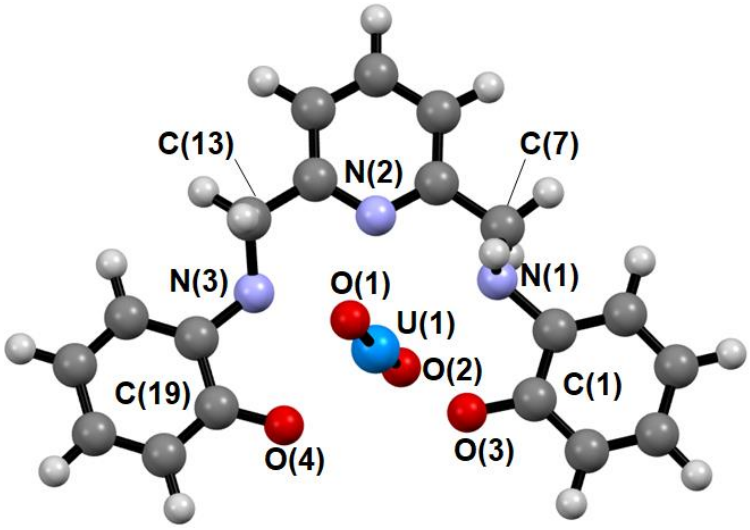

Figure S27. The DFT-optimized structures of **1**. The *tert*-butyl groups replaced by hydrogens. Selected bond lengths (Å): U(1)−O(1) 1.798, U(1)−O(2) 1.798, U(1)−O(3) 2.271, U(1)−O(4) 2.271, U(1)−N(1) 2.672, U(1)−N(2) 2.626, U(1)−N(3) 2.672, C(1)−O(3) 1.327, C(19)−O(4) 1.327, C(7)−N(1) 1.477, C(13)−N(3) 1.477.

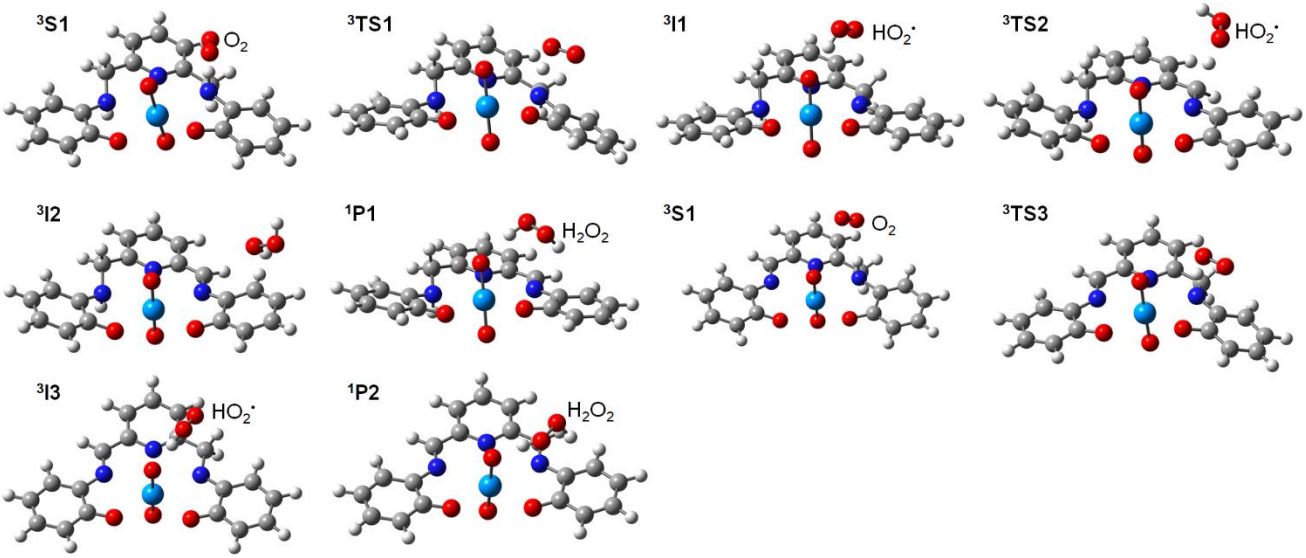

Figure S28. The structures of **S, TS**, **I, P** shown in Figure 8.

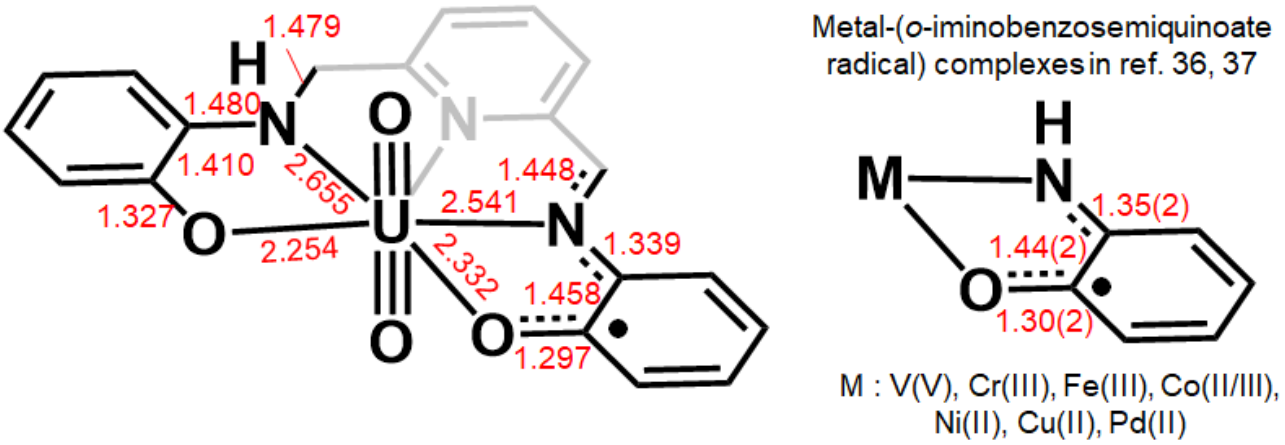

Figure S29. Selected bond lengths of **^{3}I1** shown in Figure 8 and metal-(*o*-iminobenzosemiquinoate radical) complexes reported previously.